Electrochimica Acta 571 (2026) 149128

Contents lists available at ScienceDirect

Electrochimica Acta

journal homepage: www.journals.elsevier.com/electrochimica-acta

Electrochemically tunable 2D supramolecular networks from cyclic triimidazole on Au(111)

Francesco Cazzadori [a], Daniel Forrer [a,b], Elena Lucenti [c], Elena Cariati [c,d], Christian Durante [a,*]

[a] Department of Chemical Sciences, University of Padova, via Marzolo 1, Padova 35131, Italy
[b] CNR-ICMATE, via Marzolo 1, Padova 35131, Italy
[c] Institute of Chemical Sciences and Technologies "Giulio Natta" SCITEC of CNR, via Golgi 19, 20133 Milano, Italy
[d] University of Milan, Department of Chemistry, via Golgi 19, 20133 Milano, Italy

ARTICLE INFO

Keywords:
EC-STM
Cyclic triimidazole
Au(111)
Self-assembly
Electrochemistry

ABSTRACT

Two-dimensional supramolecular networks obtained from the self-assembly of simple unit block called tectons draw a considerable interest as novel functional materials for various fields of application, such as sensing, electrocatalysis and microelectronics. The key advantages of these systems concern the precise control over the local chemical environment by tecton design and the reversible response to external stimuli such as the applied voltage. Electrochemical Scanning Tunneling Microscopy (EC-STM) allows to characterize the supramolecular geometry in real-world operating conditions and when combined with Cyclic Voltammetry analysis, it helps to investigate the role of fundamental interactions in the supramolecular network behavior.

This study presents an EC-STM/CV/DFT analysis of cyclic triimidazole self-assembly on Au(111) at electrode/electrolyte interphase. Cyclic Triimidazole (TT) is shown to form a self-assembled monolayer on Au(111) when the substrate is interfaced with a 0.1 M $HClO_4$ + 0.1 mM TT electrolytic solution. The so-formed supramolecular monolayer reveals a P6 group symmetry impressed by intermolecular N··H hydrogen bonds between TT tectons and confirmed by DFT calculations. This adlayer retains the same geometry in a wide potential window, which is limited, at 0.2 V vs RHE, by a potential-induced reversible phase transition and, at 0.95 V vs RHE, by an oxidation process with the formation of a disordered layer with a passivating effect on the gold substrate. The key advance is the identification of a cyclic triimidazole network at an electrified Au(111)/aqueous interface, with remarkable structural stability across a wide potential range. Therefore, this work bridges UHV studies of TT self-assembly with electrochemical conditions, offering a more realistic picture of interfacial supramolecular organization.

1. Introduction

Molecular adsorption and self-assembly at metal surfaces is a nanotechnological tool that enables the synthesis of a plethora of novel functional two-dimensional materials with various applications ranging from electrochemical sensing [1], heterogeneous electrocatalysis [2–6], corrosion protection [7,8] and microelectronics [9,10]. In the microelectronic field, self-assembled monolayers are gaining a renewed interest, since they provide a further level of miniaturization if compared with nanolithography techniques. Furthermore, they possess peculiar optical properties exploitable in quantum computing devices and neuromorphic devices [11–13]. The interest for 2D molecular systems is also growing in the heterogeneous electrocatalysis field, where they are employed not only as highly performing electrocatalysts, but also as model systems helping to unravel the reactivity of different active sites and rationalize it by building reactivity scales, while keeping the authentic heterogeneous conditions [14,15].

A detailed knowledge of the interactions that guide the formation of self-assembled monolayers over single crystalline surfaces is fundamental to fine tune the supramolecular adlayer in terms of geometry and local chemical environment. Those interactions can be distinguished into two main components: the vertical adsorbate-substrate interaction and the lateral adsorbate-adsorbate one. They can be of different types, ranging from more isotropic interactions such as van der Waals and Coulomb ones, to more directional ones such as hydrogen bonds, halogen bonds, metallo-ligand bonds, etc. [16]. The interplay between

* Corresponding author.
E-mail address: christian.durante@unipd.it (C. Durante).

https://doi.org/10.1016/j.electacta.2026.149128
Received 24 February 2026; Received in revised form 10 May 2026; Accepted 15 May 2026
Available online 16 May 2026

them determines the final geometry of the adlayer and its response to external stimuli such as temperature, light, and voltage variations [17]. In particular, voltage variations can be rapidly applied and precisely controlled by the imposed potential in an electrochemical system, which then is suitable for the Electrochemical Scanning Tunneling Microscopy (EC-STM) investigation. The high electric field building up at the solid-liquid electrified interface as a function of the applied potential is in the order of 10^9 V m^{-1}. However, its influence on the molecular adlayer ultimately depends on the net charge carried by the molecules; indeed, it can become irrelevant in some cases, such as with neutral and nonpolar molecules, resulting in the same geometry for electrolytic and vacuum interfaces. In other cases, several potential-induced phenomena can occur: electrocompression, electrorelaxation, phase changes, intercalation, desorption, adsorption and chemisorption [18].

EC-STM is one of the most suitable techniques to investigate molecular adlayers at the electrified interface for its single atom resolution combined with in situ and operando measurements. The supramolecular geometry of the adlayer and its dynamic response to the applied potential can be discerned [19]. The precise orientation of the adsorbed molecules within the self-assembled adlayer and with respect to the substrate can be directly determined, while the chemical composition of the adlayer can be indirectly inferred [20,21].

In this work, we employ the insightful EC-STM characterization tool to explore the self-assembly of Cyclic Triimidazole (TT, Fig. 1) on Au (111) single crystal in 0.1 M $HClO_4$ electrolyte, where Au(111) serves as the electrode support and enables precise control of the electrode potential. This class of organic compounds and its derivatives have a recent story since TT was firstly isolated in 1973 [22], but a convenient synthetic procedure was developed only in 2011 [23]. For this reason, studies on TTs are still limited even though Forni et al., highlighted their intriguing properties and potential as versatile tectons for the bottom-up synthesis of new materials [24]. It should be noted that the STM investigation of this system is limited to the TT self-assembled adlayer on Ag(111) in Ultra-High Vacuum (UHV) conditions [25]. However, UHV is an extreme condition that is far from real-world applications. In fact, exposing the molecular monolayer to atmospheric pressure and interfacing it with other materials is a necessary step to fabricate sensors, catalysts, or microelectronic devices. This step, however, does not guarantee the preservation of the monolayer, as external perturbations, such as competitive adsorption of interfaced species or interfacial potentials, can disrupt the equilibrium of the adlayer. This is why we consider the challenging possibility of studying TT at the electrode-electrolyte interface particularly valuable: it allows us to explore a more realistic scenario in which the two-dimensional adlayer can be utilized and to gain a better understanding of the interactions responsible for the formation of this supramolecular layer. Therefore, the novelty of this work lies not simply in the self-assembly of TT, but in the direct resolution of a cyclic triimidazole network at an electrified Au (111)/aqueous interface, demonstrating its structural persistence over a broad potential window. By bridging previous UHV-based supramolecular studies of TT with realistic electrochemical environments, this study provides a more application-relevant understanding of interfacial self-assembly and refines the current conceptual framework.

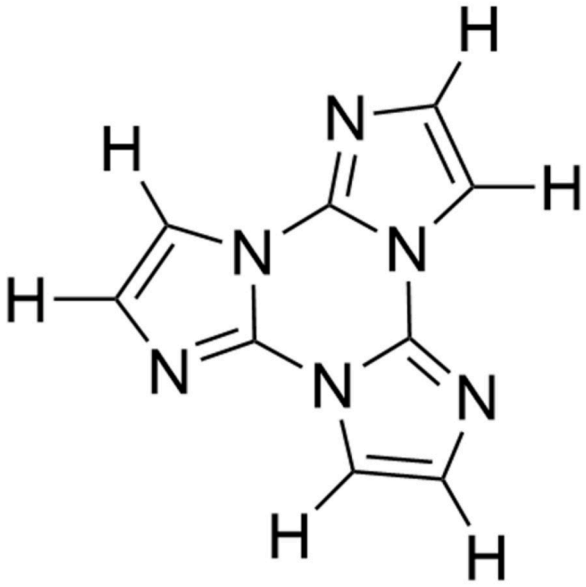

Fig. 1. Cyclic triimidazole molecular structure.

2. Experimental

2.1. Chemicals, materials, and procedures

TT was prepared as described in the literature [23], and purified by recrystallization. N,N-dimethylformamide (HPLC grade, Sigma-Aldrich) was used to prepare a 0.1 mM TT solution. Perchloric acid (TraceSELECT Ultra, Fluka) was diluted with Millipore Milli-Q water (resistivity $\geq$ 18.2 MΩ·cm, TOC $\leq$ 5 ppb) to obtain a 0.1 M solution, and TT was added to the resulting electrolyte to a final concentration of 0.1 mM. Hat-shaped Au(111) single crystal with orientational accuracy $<0.1^\circ$ and 99.999% purity was purchased from MaTeck. The flame annealing of the single crystal, 3 min with a butane air torch, was performed every day to restore the substrate surface before the functionalization step. The functionalization of Au(111) was carried out with two alternative methods. In the first, the crystal surface was brought into contact with a hanging meniscus of a 0.1 mM TT solution in DMF, followed by rinsing with water and subsequent immersion in the 0.1 M $HClO_4$ electrolyte in the electrochemical cell. In the second method, TT powder was dissolved directly in the electrolyte to a final concentration of 0.1 mM. The laboratory glassware was always accurately cleaned with Piranha solution (H_2SO_4/H_2O_2 1/1) and washed three times with Milli-Q water in the ultrasonic bath prior to use.

2.2. Electrochemical methods

A home-built Wandelt type EC−STM was employed [26]. The custom EC-STM electrochemical cell was machined from a PEEK tube. The working electrode (WE) was sealed to the cell by pressing it against an O-ring, while both the counter electrode (CE) and the pseudoreference electrode (RE) were platinum wires. The pseudoreference electrode was calibrated against the reversible hydrogen electrode (RHE) in 0.1 M $HClO_4$ aqueous electrolyte and the following conversion value was measured: E_{Pt} = 0.85 V vs RHE. The electrochemical cell was placed inside the EC-STM Faraday cage, with a sealed enclosure to maintain a controlled atmosphere. Images were acquired by recording the topographical signal in constant-current mode, in which a defined tunneling current setpoint (I_t) was maintained. Additionally, a fixed bias voltage between the tip and the working electrode (U_b) and a controlled potential between the working and reference electrodes (E_{WE}) were applied using the EC-STM bipotentiostat. Acquired images were filtered with a python-based automated procedure [27] and analyzed with the WSxM software [28]. Potentiodynamic EC-STM experiments were mainly performed by manually sweeping the potential in the time interval between consecutive images. In few specified cases the potential was changed during the image acquisition, a manual sweep was performed to produce an EC-STM image where the upper part is at the initial potential, the middle part is the potential variation zone, and the bottom part is at the final potential. These regions were not outlined in the image reported here because the surface microscopic phenomena, related to the presented potential variations, produce sharp image variations, hence becoming an internal label of the imposed potential variation. The rate of the potential sweep performed manually was approximately 20 mV/s in the time frame between images and 60 mV/s

when varied during the image acquisition. EC-STM tips were fabricated from 0.25 mm straight tungsten wire and etched using the drop-off method in 2 M KOH. The tips were then rinsed with Milli-Q water and ethanol and dried in air. Finally, the upper portion of each tip was coated with hot-melt glue to form an electrically insulating layer, preventing the occurrence of faradaic currents when the tip was immersed in the electrolyte.

Cyclic voltammetry (CV) was performed either in situ, using the EC-STM cell, or ex situ, in a standard three-electrode glass cell. The in situ configuration allows electrochemical characterization of the sample during STM image acquisition, albeit with a less precise reference electrode (RE) and a longer preparation procedure. In contrast, the ex situ setup requires shorter preparation times and allows the use of a stable reversible hydrogen electrode (RHE) as RE. The RHE was constructed from a spiral of Pt wire mounted at the closed end of a glass capillary; prior to each experiment, the electrode was filled with electrolyte and H_2 was generated electrochemically at the Pt wire via chronoamperometry until approximately half of the spiral was filled with gas. In situ measurements were performed using the EC-STM bipotentiostat coupled with a Wenking MVS 98 scan generator, while ex situ measurements were carried out with a Gamry Interface 1010E potentiostat.

2.3. Computational modelling

Density Functional Theory (DFT) calculations were performed using Quantum-Espresso (QE) [29]. Wavefunctions were expanded over a plane-wave basis set with 40 Ry cutoff, while the cutoff in density was 400 Ry. Ultrasoft pesudopotentials of the GBRV library [30] were employed. The PBE [31] approximation to the exchange-correlation functional was used and corrected for dispersion interactions using the DFT-D2 formula [32], as implemented in QE [33]. The overlayer structure was optimized using a variable-cell algorithm until the stress was lower than 0.5 kbar and forces acting on atoms were lower than 10–3 Ry/bohr. The distance between replicas along the z direction was 20 Å.

3. Results and discussions

3.1. EC-STM investigation

The Au(111) surface prior to functionalization exhibits the typical

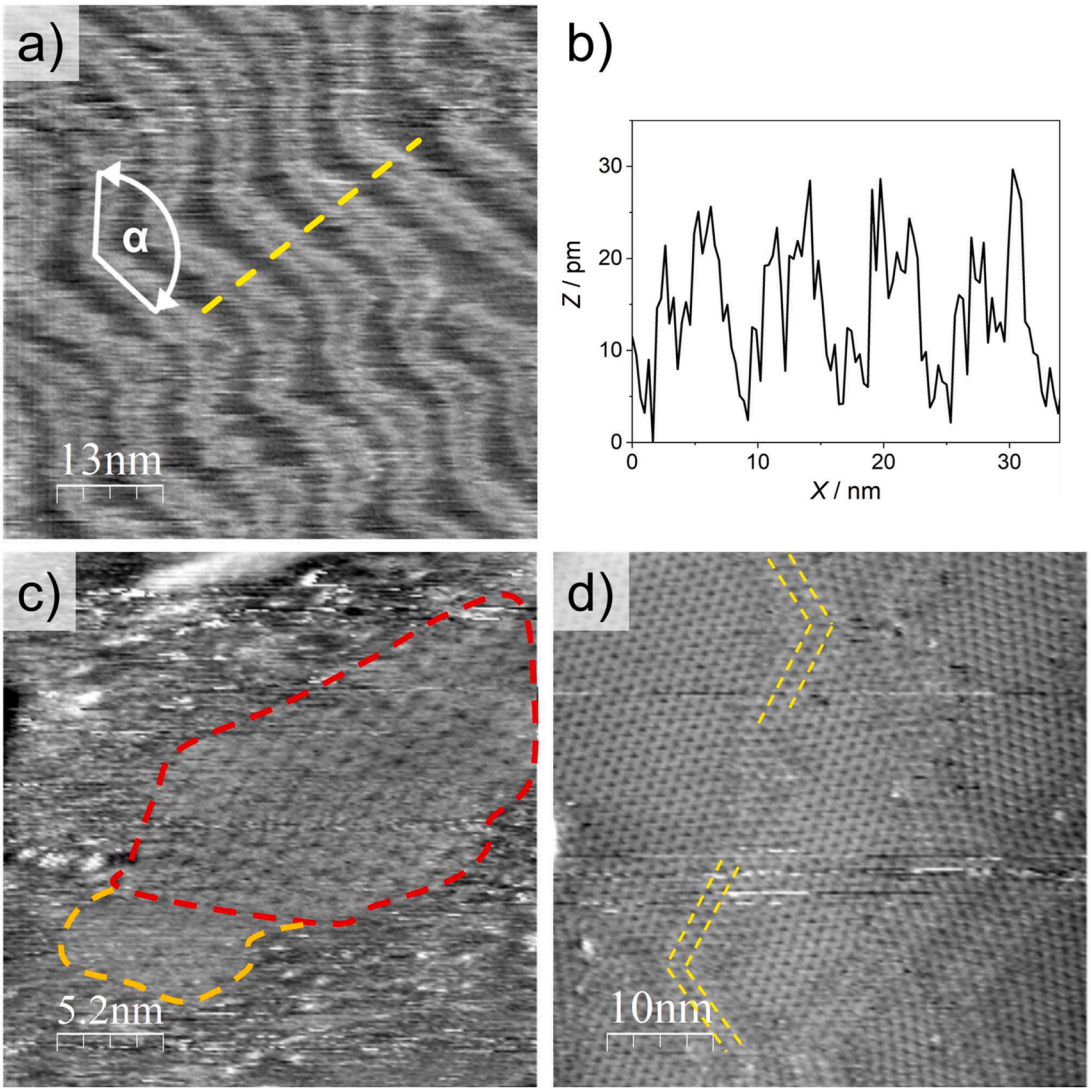

Fig. 2. a) EC−STM image of bare Au(111) in Air with a topographic profile b) traced perpendicular to the herringbone reconstruction stripes; tunneling conditions: I_t = 1.6 nA, U_b = −400 mV; c-d) EC−STM images in aqueous electrolyte saturated with Ar: c) TT@Au(111) in contact with 0.1 M $HClO_4$ electrolyte, tunneling conditions: I_t = 1 nA, U_b = −200 mV, E_{WE} = −350 mV; d) Au(111) in contact with 0.1 M $HClO_4$ + 0.1 mM TT electrolyte, tunneling conditions: I_t = 1.6 nA, U_b = −300 mV, E_{WE} = −350 mV, the dashed lines follow the herringbone reconstruction pattern extending underneath the TT monolayer.

herringbone reconstruction (Fig. 2a). The topographic dimensions of the reconstruction agree with previous studies [34,35]; the elbow internal angle is (122 ± 5)°, the height of the roughened striped pattern is around 20 pm and the distance between repeating stripes is 7 nm (Fig. 2b). The functionalization with TT results in a self-assembled molecular monolayer exhibiting a hexagonal geometry. As reported in literature [25], under UHV conditions, TT produces a triangular-shaped contrast in STM images and organizes into hexagonal supramolecular domains. However, in an electrochemical environment, the stability of the layer is influenced by additional factors, including temperature, pressure, and, last but not least, the electrolyte. In fact, continuous dissolution of the adsorbate affects the stability of the adlayer, leading to a rapid transition from a fully covered surface to one exhibiting only small, fragmented domains. Fig. 2c shows a small, isolated domain outlined with a dashed red line. The adjacent region, outlined in orange, corresponds to a fragment of the domain undergoing desorption, which appears as a cloudy area in the EC-STM image. This desorption process could be promoted by the slight solubility of TT in water [36]. Therefore, to improve the stability of the adlayer, a small concentration of TT (0.1 mM) was also added to the electrolyte, allowing the spontaneous formation of a self-assembled monolayer on the Au(111) surface (Fig. 2d). In this condition it is possible to distinguish the herringbone reconstruction pattern extending beneath the TT monolayer (yellow dashed lines in Fig. 2d). Compared to the bare Au(111), where the herringbone reconstruction stripes in the STM image are densely packed together, the stripes are more straggled in the presence of the TT adlayer (dashed lines in Fig. 2d). The perturbation of the herringbone reconstruction can be an index of the vertical interaction strength between the adsorbed molecule and the Au(111) substrate [37]. In the case of TT, the three aromatic cycles provide a source of π-metal vertical interactions. The partial lifting of the herringbone together with the spontaneous desorption of TTs could be motivated by a not strong enough interaction with the gold substrate.

High resolution EC−STM images, such as the one displayed in Fig. 3a, reveal in detail the structure of the self-assembled TT adlayer. The individual molecular unit adsorbs in a planar configuration on the Au(111) giving a triangular shaped response, where the bright dots at the triangle vertices corresponds to a local increase of the tunneling signal provided by the aromatic imidazole centers. The primitive unit cell, outlined in Fig. 3b, pertains to the P6 space group, where the TT units are centered on the threefold axes, the hydrogen bonds on the twofold axes and the empty spaces on the sixfold axes. The primitive unit base vectors were measured to be $a = b = (1.28 \pm 0.06)$ nm and internal angle $\alpha = (120 \pm 2)°$. Therefore, the surface concentration of TT is estimated to be $\sigma_{TT} = 1.41 \cdot 10^{14}$ molecules cm^{-2}. An interesting aspect is the similarity between this adlayer and previous results obtained by Ahsan et al. for TT self-assembly on Ag(111) in UHV. In their study, the authors have observed not only the same triangular shaped response for the TT molecule but also similar values for the primitive unit cell, only smaller by ≈0.1 nm [25]. This similarity between adlayers on different substrates underlines the key role of lateral interactions between TT molecules, provided by hydrogen bonds, to determine the final self-assembly geometry. Nevertheless, the simultaneous presence of π-metal interactions cannot be discarded, and they are also a driving force in the adlayer formation, even if with a minor contribution.

In Fig. 3c the modelling of the molecular overlayer is represented. A hexagonal cell with P6 symmetry was employed. The DFT-optimized structure has a cohesion energy of −0.43 eV per TT unit and is characterized by a N··H distance of 2.22 Å, compatible with the formation of the hydrogen bond network. This leads to a cell parameter of 1.34 nm, which is consistent with the experimental value. The density of the HOMO is delocalized over the whole TT and is characterized by a threefold symmetric nodal structure at the central ring, compatible with the dimmer contrast of the molecular core observed at the EC−STM.

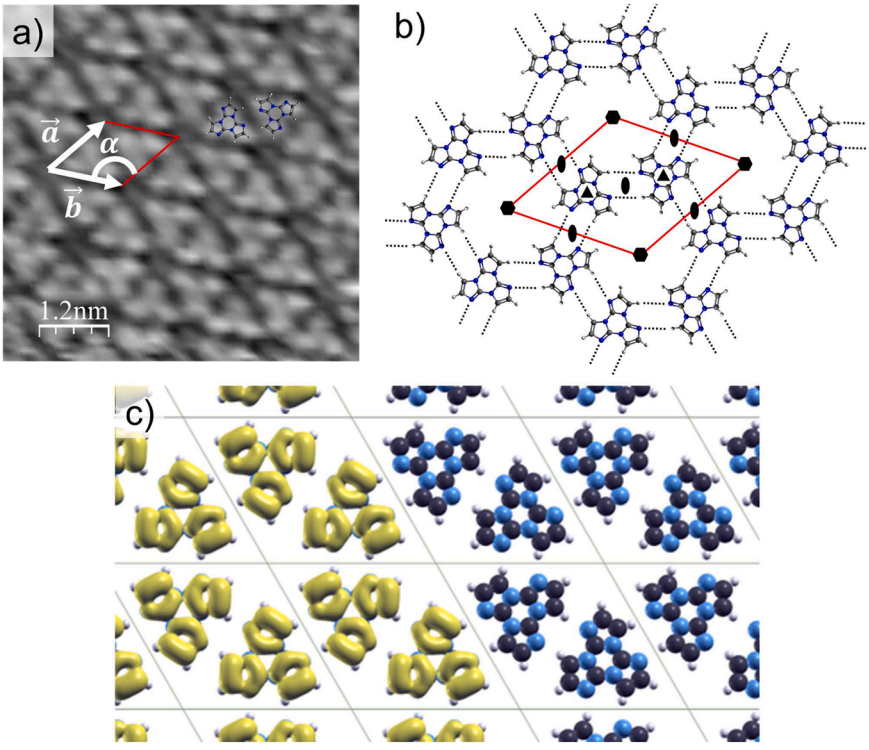

Fig. 3. a) High resolution EC−STM image of the TT@Au(111) adlayer, tunneling conditions: $I_t = 2.3$ nA, $U_b = -200$ mV, $E_{WE} = -350$ mV; b) adlayer structure model with the primitive cell outlined in red and the symmetry elements of the P6 space group reported in black; c) optimized adlayer geometry obtained from DFT calculations with the HOMO density on the left side exhibiting a threefold symmetric nodal structure at the central ring. Color code in atomic models: C dark gray, N blue, H white.

3.2. Cyclic voltammetry investigation

The electrochemical response of the self-assembled adlayer is investigated in Fig. 4. A comparison of the voltammograms of Au(111) recorded in deaerated 0.1 M $HClO_4$ before and after the addition of 0.1 mM TT to the supporting electrolyte (Fig. 4a,b) reveals several notable changes. In Fig. 4a) a reversible redox couple emerges at 0.2 V vs RHE, the herringbone lifting redox couple (≈ 0.8 V vs RHE) exhibits an approximately one-third decrease in peak intensity and a cathodic shift of 50 mV and the interfacial capacitance is reduced by roughly one-half. In Fig. 4b) the Au(111) oxidation wave is markedly attenuated and shifted toward more positive potentials, and the gold reduction peak is correspondingly diminished in the reverse scan. The redox properties of TT were previously investigated by Magni et al. under homogeneous conditions at a glassy carbon electrode and in dimethylformamide and tetrabutylammonium hexafluorophosphate as the supporting electrolyte [38]. In that study, the electrochemical response of TT reveals sluggish redox activity: both the reduction and oxidation peaks occur near the

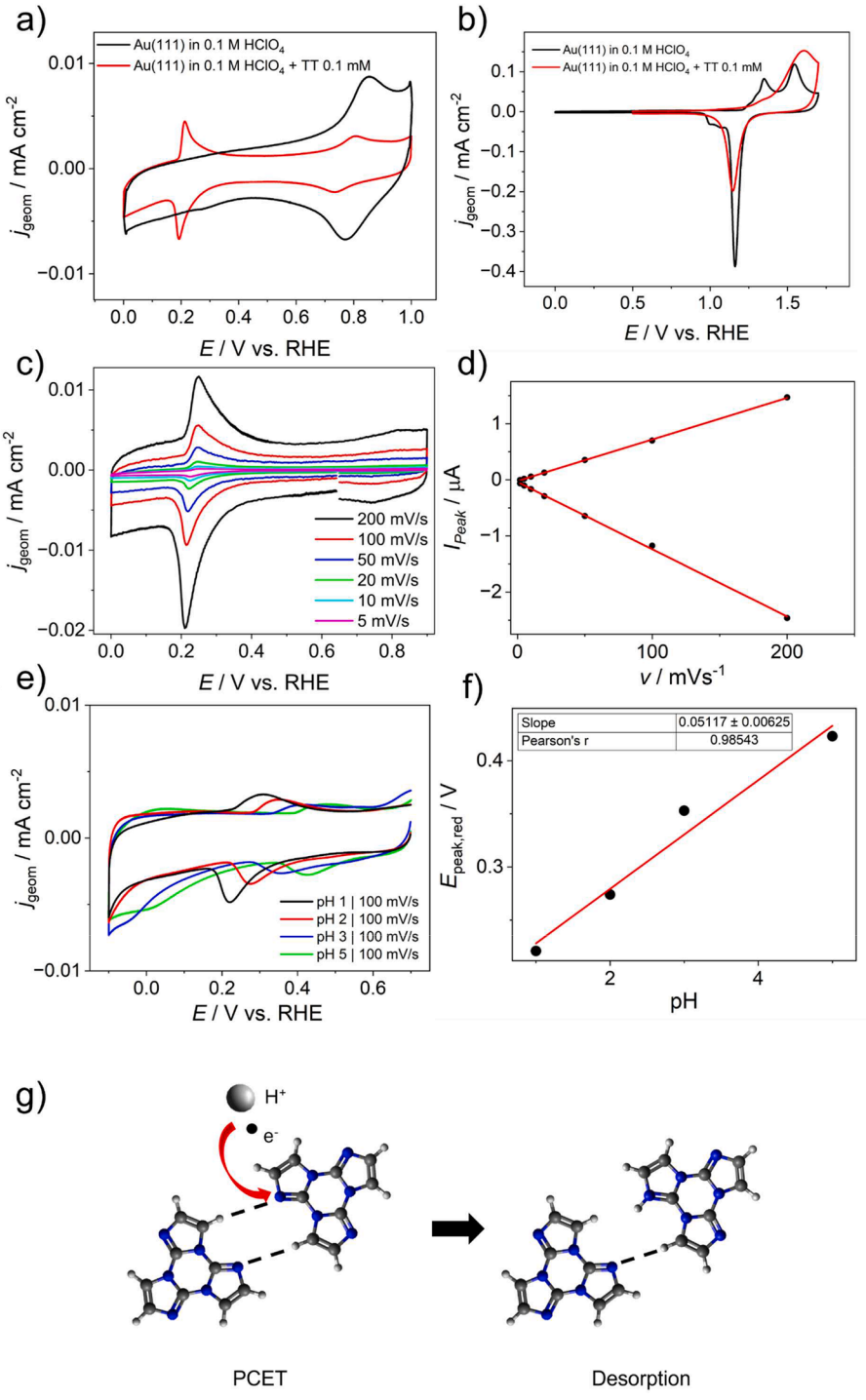

Fig. 4. CV investigation; a,b) comparison of the CV response in deaerated atmosphere of Au(111) in 0.1 M $HClO_4$ (black line) and Au(111) in 0.1 M $HClO_4$ + 0.1 mM TT (red line); c) CVs at different scan rates of Au(111) in 0.1 M $HClO_4$ + 0.1 mM TT; d) linear fit of the reduction and oxidation peak currents versus the scan rate; e) CVs at different pH values of Au(111) in 0.1 M $NaClO_4$ + 0.1 mM TT; f) linear fit of the reduction peak current versus the pH; g) proposed mechanism for the potential-induced desorption of the TT adlayer.

limits of the accessible potential window and are associated with irreversible redox processes leading to the formation of a radical anion and a radical cation, respectively. Therefore, the redox couple observed at 0.2 V vs RHE is unlikely to originate from the formation of the TT radical anion due to the mild potential at which the redox process occurs. Moreover, in acidic aqueous electrolyte, the pyridine-like nitrogen of the TT molecule is expected to be partially protonated at the pH employed in Fig. 4a, given its reported pK_a of 1.5 [39]. To further investigate this redox process from the CV point of view, the effect of pH on the potentials of the TT reduction and oxidation peaks was evaluated over the pH range 1–5. The results reveal a clear pH dependence of the peak potential, with an approximate slope of 51 mV per pH unit, indicative of proton-coupled electron-transfer (PCET) behavior (Fig. 4e,f), which could be assigned to the reductive protonation of the sp^2 nitrogen in the TT. At the same time, from the EC-STM potentiodynamic measurements, that will be discussed below, the redox couple at 0.2 V vs RHE shows to be directly linked to a desorption/readsorption process of the TT adlayer. The presented evidence can be combined in a single mechanistic interpretation (Fig. 4g) considering that the PCET assumes the role of triggering step and then the resulting protonation of the sp^2 nitrogen will disrupt the hydrogen bond network leading to the desorption of the TT adlayer. This proposed mechanism is in close analogy to the behavior reported for trimesic acid adlayers [40].

The reversible peak couple that emerges in the presence of the TT adlayer exhibits the characteristic behavior of a surface-confined redox process. Specifically, upon systematic variation of the scan rate (Fig. 4c), both the anodic and cathodic peak currents display a linear dependence on the scan rate (Fig. 4d). The peak potentials vary with the scan rate, which, for a Faradaic process, would be indicative of a non-Nernstian response arising from sluggish electron-transfer kinetics. Notably, the reduction peak is the only feature that shifts appreciably, by approximately 20 mV when the scan rate is increased from 5 mV s^{-1} to 1 V s^{-1} (Figure S3). Moreover, the magnitude of the shift is more pronounced at lower scan rates than at higher ones. A similar behavior was reported by Li et al. for the redox couple of a paracyclophane monolayer formed on HOPG. In that study, the deviation from ideal Nernstian behavior was attributed to an additional chemical step following the electrochemical oxidation, leading to a transition from an adsorbed molecular monolayer to a gas-like adsorption layer [41].

3.3. Potentiodynamic investigation of TT adlayer

The influence of the TT adlayer on the herringbone reconstruction of Au(111) was investigated by combining EC-STM and CV measurements. Upon TT adsorption, EC-STM images reveal a partial lifting of the herringbone reconstruction (Fig. 2d), consistent with the decreased intensity of the peaks associated with potential-induced lifting in the CV. Moreover, the cathodic shift of these peak potentials indicates that the molecule-substrate interaction facilitates the potential-induced lifting process. The observed decrease in overall capacitance is a common effect, attributable to the formation of a molecular adlayer covering the bare Au(111) surface, as previously reported for porphyrin monolayers [42,43].

The stability of the self-assembled TT monolayer was investigated using potentiodynamic EC-STM imaging. Images were acquired while the applied potential was swept in either the cathodic or anodic direction and then returned to the starting potential. In Fig. 5, the cathodic sweep is shown alongside the cyclic voltammetry of the system, with a series of EC-STM images capturing the key events of the potential-induced phase transition. Therefore, the sequence is not intended to be an identical location experiment whereas it captures the average microscopic behavior which can then be correlated to the average macroscopic CV response. At the starting potential, chosen before the onset of the reduction peak in the CV, the TT monolayer is observed in its equilibrium state (Fig. 5b). Upon sweeping the potential beyond the reduction peak, the monolayer undergoes instantaneous desorption

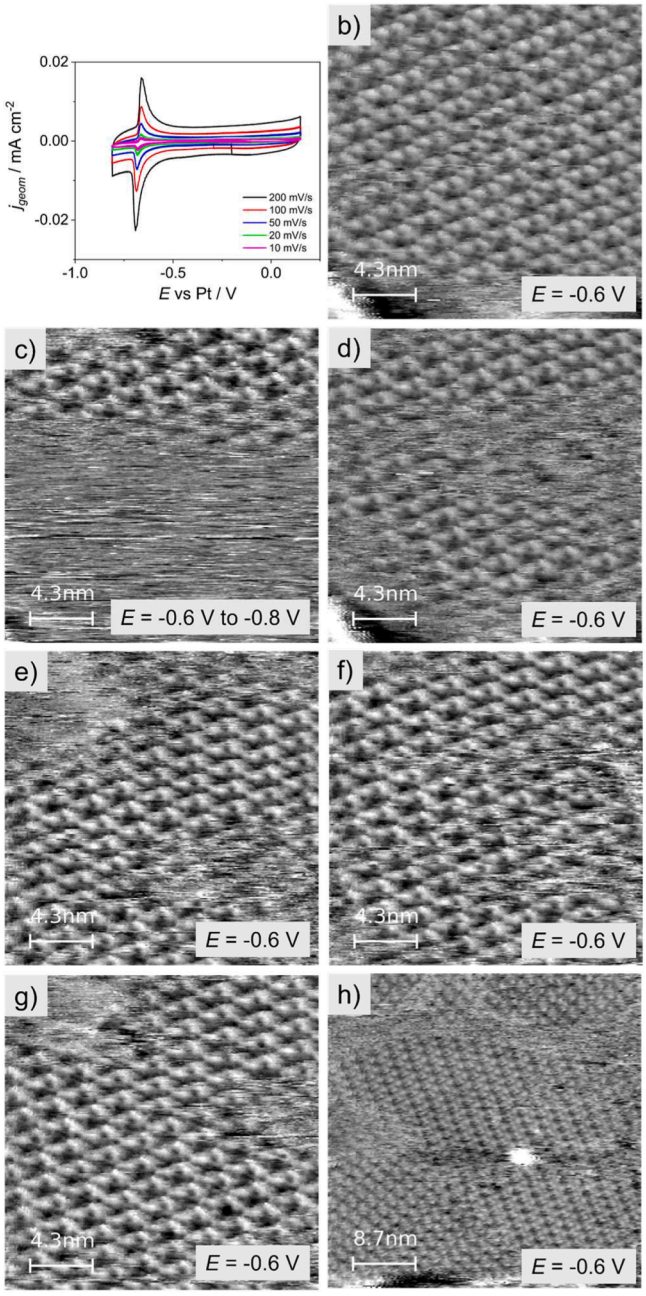

Fig. 5. EC−STM potentiodynamic image sequence (cathodic direction) of the TT@Au(111) adlayer in the electrolytic solution of 0.1 M HClO4 + 0.1 mM TT saturated with Ar; a) in situ CV of the system in the potential window of interest; the sequence starts from image b) and ends with image h), the tunneling conditions I_t = 1.6 nA and U_b = −100 mV are kept constant along the entire series except for E_{WE} which is reported in the white box at the bottom corner for every image.

(Fig. 5c). Subsequently, upon returning to the initial potential, an instantaneous reabsorption of TT takes place. The reconstructed adlayer appears fragmented into multiple orientational domains (Fig. 5d-h), with no observable variation in the periodicity of the TT molecules within individual domains. Although multiple orientational domains form even upon adsorption at the open-circuit potential (OCP) (Fig. 2d), the ones forming after the potential-induced desorption/readsorption appear smaller in size. This could be an effect of the faster adsorption dynamic which triggered by the potential sweep.

Fig. 6 presents the potentiodynamic series for the TT@Au(111) adlayer, obtained by sweeping the potential across the region of the CV

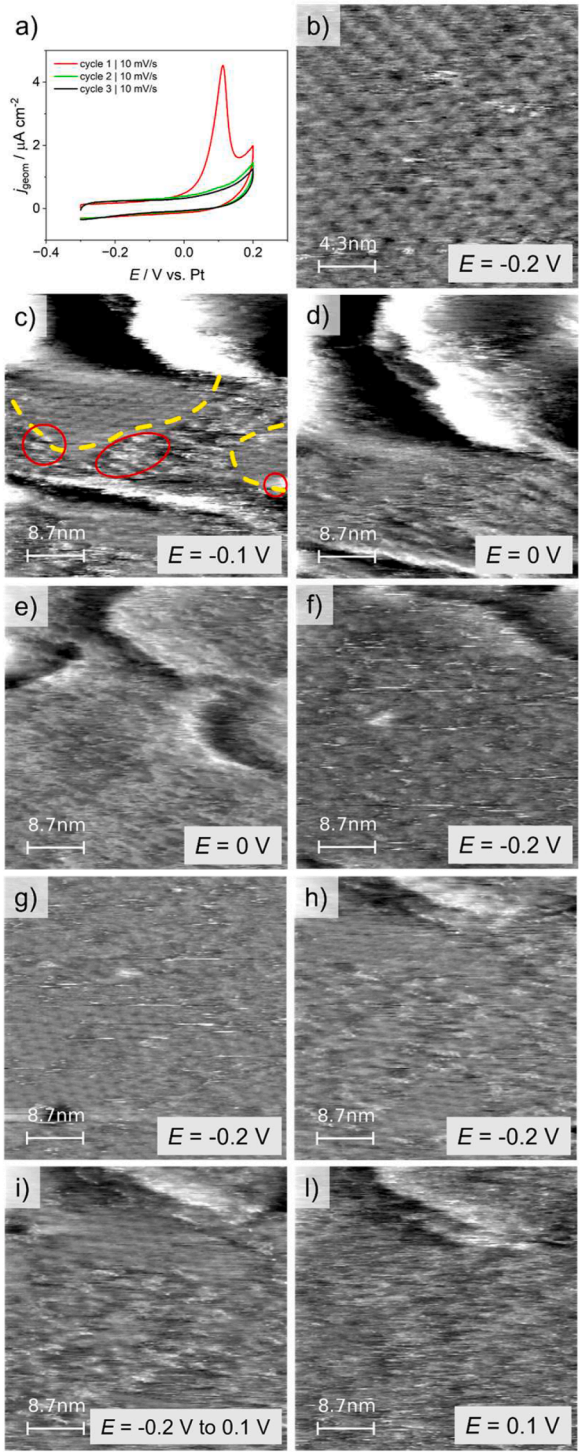

Fig. 6. EC−STM potentiodynamic image sequence (anodic direction) of the TT@Au(111) adlayer in the electrolytic solution of 0.1 M $HClO_4$ + 0.1 mM TT purged with Ar; a) in situ CV of the system in the potential window of interest; the sequence starts from image b) and ends with image l), E_{WE} is reported in the white box at the bottom corner for every image, while the tunneling conditions are the following: b) I_t = 1.6 nA and U_b = −300 mV, c-d) I_t = 2.8 nA and U_b = −500 mV, e-l) I_t = 4.1 nA and U_b = −500 mV.

shown in Fig. 6a. The voltammogram includes multiple cycles recorded at a scan rate of 10 mV s^{-1}. The peak observed only in the first cycle can be attributed to passivation of the electrode due to the formation of a disordered film of molecular aggregates visible at the EC-STM. The same voltammetric response was observed by Bardini et al. for the electrochemical polymerization of allylamine copolymers and associated to the passivation of the electrode [44]. Additionally, the hampering of the Au(111) dissolution/redeposition peaks and the onset shift of the gold oxidation wave to more positive values (Fig. 4b), are both related to electrode passivation [40,45]. Fig. 6b shows the TT adlayer in its initial ordered state at –0.2 V vs Pt, near the OCP. In Fig. 6c, the potential is increased by 100 mV, approaching the onset of the oxidation wave. Here, ordered TT domains are still visible (one outlined in yellow), while aggregates begin to form at the domain boundaries (circled in red). In Fig. 6d-e, the potential surpasses the onset, and the surface becomes completely covered by a disordered pattern of aggregates. Nonetheless, by returning to the starting potential and changing the probed location, it was still possible to find ordered TT domains with small dimensions and separated by disordered aggregates (Fig. 6f-h). Finally, a larger potential sweep from –0.2 V to +0.1 V vs Pt (Fig. 6i) results in a corresponding irreversible morphological change from the ordered TT monolayer to fully disordered aggregates. The potentiodynamic EC-STM sequence allows to correlate the formation of a disordered layer of aggregates, starting from the TT monolayer, to the oxidative peak in the related CV.

4. Conclusions

The novel cyclic triimidazole compound has proven to be a promising tecton for the formation of two-dimensional molecular monolayers at the electrode-electrolyte interface. The assembly of this supramolecular structure on Au(111) is primarily directed by intermolecular hydrogen bonding, which enforces the final P6 hexagonal geometry, rather than by π-metal interactions between the aromatic imidazole moieties and the substrate. Nonetheless, these π interactions are present and contribute to the partial lifting of the herringbone reconstruction. The resulting adlayer is stable in contact with an aqueous solution of 0.1 mM TT in 0.1 M $HClO_4$ over a broad potential range, from 0.2 V to 0.95 V vs RHE. At the cathodic limit, a potential-induced desorption and readsorption process occurs, corresponding to a reversible peak couple in the CV output. At the anodic limit, oxidation of the TT monolayer leads to the formation of a passivating, disordered layer of aggregates on the gold surface. The spontaneous self-assembly exhibited by these novel aromatic compounds offers a versatile platform for designing new supramolecular structures through controlled functionalization of TT tectons.

Data availability statement

The data are available from the corresponding author upon reasonable request.

CRediT authorship contribution statement

Francesco Cazzadori: Writing – original draft, Methodology, Investigation. **Daniel Forrer:** Investigation, Data curation. **Elena Lucenti:** Investigation. **Elena Cariati:** Investigation, Conceptualization. **Christian Durante:** Writing – review & editing, Supervision, Resources, Project administration, Conceptualization.

Declaration of competing interest

The authors declare that they have no known competing financial interests or personal relationships that could have appeared to influence the work reported in this paper.

Acknowledgements

The University of Padova and the Chemical Sciences Department are gratefully acknowledged for the P-DISC Grant PROMETEO (project number: P-DiSC#03NExuS_BIRD2021-UNIPD). MIUR is also

acknowledged for the support to the project financed by the European Community— Next Generation EU—Bando PRIN 2022 PNRR—M4. C2.1.1: Progetto: P2022WANKS—ECHO-EF.

Supplementary materials

Supplementary material associated with this article can be found, in the online version, at doi:10.1016/j.electacta.2026.149128.

References

[1] D. Mandler, S. Kraus-Ophir, Self-assembled monolayers (SAMs) for electrochemical sensing, J. Solid. State Electrochem. 15 (2011) 1535–1558, https://doi.org/10.1007/s10008-011-1493-6.

[2] J.J. Gammelgaard, Z. Sun, A.K. Vestergaard, S. Zhao, Z. Li, N. Lock, K. Daasbjerg, A. Bagger, J. Rossmeisl, J.V. Lauritsen, A monolayer carbon nitride on Au(111) with a high density of single Co sites, ACS. Nano 17 (2023) 17489–17498, https://doi.org/10.1021/acsnano.3c05996.

[3] N. Arisnabarreta, Y. Hao, E. Jin, A. Salamé, K. Muellen, M. Robert, R. Lazzaroni, S. Van Aert, K.S. Mali, S. De Feyter, Single-layered imine-linked porphyrin-based two-dimensional covalent organic frameworks targeting CO2 reduction, Adv. Energy Mater. 14 (2024) 2304371, https://doi.org/10.1002/aenm.202304371.

[4] F. Cazzadori, A. Facchin, S. Reginato, D. Forrer, C. Durante, Free-base octaethylporphyrin on Au(111) as heterogeneous organic molecular electrocatalyst for oxygen reduction reaction in acid Media: an electrochemical scanning tunneling microscopy and rotating ring-disc electrode analyses, Small. Sci. 5 (2025) 2400294, https://doi.org/10.1002/smsc.202400294.

[5] A. Facchin, T. Kosmala, A. Gennaro, C. Durante, Electrochemical scanning tunneling microscopy investigations of FeN4-based macrocyclic molecules adsorbed on Au(111) and their implications in the oxygen reduction reaction, Chem. Electrochem. 7 (2020) 1431–1437, https://doi.org/10.1002/celc.202000137.

[6] A. Facchin, M. Zerbetto, A. Gennaro, A. Vittadini, D. Forrer, C. Durante, Oxygen reduction reaction at single site catalysts : a combined electrochemical scanning tunnelling microscope and DFT investigation of iron octaethylporphyrin chloride on HOPG, Chem. Electrochem. (2021) 1–10.

[7] M.R. Vogt, R.J. Nichols, O.M. Magnussen, R.J. Behm, Benzotriazole adsorption and inhibition of Cu(100) corrosion in HCl: a combined in situ STM and in situ FTIR spectroscopy study, J. Phys. Chem. B 102 (1998) 5859–5865, https://doi.org/10.1021/jp981216e.

[8] S. Ramachandran, B.-L. Tsai, M. Blanco, H. Chen, Y. Tang, W.A. Goddard, Self-assembled monolayer mechanism for corrosion inhibition of iron by imidazolines, Langmuir. 12 (1996) 6419–6428, https://doi.org/10.1021/la960646y.

[9] Z. Chen, S. Duan, X. Zhang, W. Hu, Novel solution-processed 2D organic semiconductor crystals for high-performance OFETs, Mater. Chem. Front. 8 (2024) 2227–2272, https://doi.org/10.1039/D3QM01281F.

[10] C.T. Black, R. Ruiz, G. Breyta, J.Y. Cheng, M.E. Colburn, K.W. Guarini, Polymer self assembly in semiconductor microelectronics, IBM. J. Res. Dev. 51 (2007) 605–633, https://doi.org/10.1147/rd.515.0605.

[11] L. Ai, Y. Pei, Z. Song, X. Yong, H. Song, G. Liu, M. Nie, G.I.N. Waterhouse, X. Yan, S. Lu, Ligand-triggered self-assembly of flexible carbon dot nanoribbons for optoelectronic memristor devices and neuromorphic computing, Adv. Sci. 10 (2023) 2207688, https://doi.org/10.1002/advs.202207688.

[12] F.F. Lupi, G. Milano, A. Angelini, M. Rosero-Realpe, I. Murataj, B. Torre, E. Cara, P. Hönicke, A. Wählisch, E. Kozma, D. Antonioli, M. Laus, A. Motta, C. Martella, C. Grazianetti, Enhanced photoluminescence in a neuromorphic 2D memitter based on WS_2 via plasmonic nanoparticle self-assembly, ACS. Appl. Mater. Interfaces. 17 (2025) 35695–35704, https://doi.org/10.1021/acsami.5c03059.

[13] D.V. Talapin, M. Engel, P.V. Braun, Functional materials and devices by self-assembly, MRS Bull. 45 (2020) 799–806, https://doi.org/10.1557/mrs.2020.252.

[14] A. Facchin, C. Durante, Metal porphyrins as single site catalyst models explored by electrochemical scanning tunneling microscopy: a new perspective in electrocatalysis, Advanced Sustainable Systems 2200111 (2022). https://doi.org/10.1002/adsu.202200111.

[15] A. Facchin, D. Forrer, M. Zerbetto, F. Cazzadori, A. Vittadini, C. Durante, Single-site catalysts for the oxygen reduction reaction: why iron is better than platinum, ACS. Catal. 14 (2024) 14373–14386, https://doi.org/10.1021/acscatal.4c02366.

[16] A. Ciesielski, C.-A. Palma, M. Bonini, P. Samorì, Towards supramolecular engineering of functional nanomaterials: pre-programming multi-component 2D self-assembly at solid-liquid interfaces, Adv. Mater. 22 (2010) 3506–3520, https://doi.org/10.1002/adma.201001582.

[17] Z. Li, Y. Li, C. Yin, Manipulating molecular self-assembly process at the solid–Liquid interface probed by scanning tunneling microscopy, Polymers. (Basel) 15 (2023) 4176, https://doi.org/10.3390/polym15204176.

[18] S.F.L. Mertens, Adsorption and self-organization of organic molecules under electrochemical control. Encyclopedia of Interfacial Chemistry, Elsevier, 2018, pp. 13–23, https://doi.org/10.1016/B978-0-12-409547-2.13061-6.

[19] C. Leasor, K.-H. Chen, T. Closson, Z. Li, Revealing the structural complex of adsorption and assembly of benzoic acids at electrode–Electrolyte interfaces using electrochemical scanning tunneling microscopy, J. Phys. Chem. C 123 (2019) 13600–13609, https://doi.org/10.1021/acs.jpcc.9b01705.

[20] B. Xu, S. Yin, C. Wang, Q. Zeng, X. Qiu, C. Bai, Identification of hydrogen bond characterizations of isomeric 4Bpy and 2Bpy by STM, Surf. Interface Anal. 32 (2001) 245–247, https://doi.org/10.1002/sia.1046.

[21] M. Lackinger, W.M. Heckl, Carboxylic acids: versatile building blocks and mediators for two-dimensional supramolecular self-assembly, Langmuir. 25 (2009) 11307–11321, https://doi.org/10.1021/la900785f.

[22] K.L. Kirk, W. Nagai, L.A. Cohen, Photochemistry of diazonium salts. II. Synthesis of 2-fluoro-L-histidine and 2-fluorohistamine, and the halogen lability of 2-fluoroimidazoles, J. Am. Chem. Soc. 95 (1973) 8389–8392, https://doi.org/10.1021/ja00806a031.

[23] D.M. Schubert, D.T. Natan, D.C. Wilson, K.I. Hardcastle, Facile synthesis and structures of cyclic triimidazole and its boric acid adduct, Crystal Growth Design 11 (2011) 843–850, https://doi.org/10.1021/cg101489t.

[24] A. Forni, D. Malpicci, D. Maver, E. Lucenti, E. Cariati, The intriguing case of cyclic triimidazole: an emerging scaffold for the preparation of multiemissive, biomedical and hybrid inorganic–organic materials, J. Mater. Chem. C 13 (2025) 3721–3758, https://doi.org/10.1039/D4TC04766D.

[25] A. Ahsan, X. Wang, R. Sk, M. Heydari, L. Buimaga-Iarinca, C. Wäckerlin, E. Lucenti, S. Decurtins, E. Cariati, T.A. Jung, U. Aschauer, S.-X. Liu, Self-assembly of N-rich triimidazoles on Ag(111): mixing the pleasures and pains of epitaxy and strain, J. Phys. Chem. C 127 (2023) 23000–23009, https://doi.org/10.1021/acs.jpcc.3c03325.

[26] M. Wilms, M. Kruft, G. Bermes, K. Wandelt, A new and sophisticated electrochemical scanning tunneling microscope design for the investigation of potentiodynamic processes, Rev. Sci. Instrum. 70 (1999) 3641–3650, https://doi.org/10.1063/1.1149971.

[27] F. Cazzadori, A. Facchin, S. Reginato, C. Durante, Simple Python-based methods for analysis and drift-correction of STM images, J. Microsc. 302 (2026) 39–49, https://doi.org/10.1111/jmi.13426.

[28] I. Horcas, R. Fernández, J.M. Gómez-Rodríguez, J. Colchero, J. Gómez-Herrero, A. M. Baro, WSXM: a software for scanning probe microscopy and a tool for nanotechnology, Rev. Sci. Instrum. 78 (2007) 013705, https://doi.org/10.1063/1.2432410.

[29] P. Giannozzi, O. Andreussi, T. Brumme, O. Bunau, M. Buongiorno Nardelli, M. Calandra, R. Car, C. Cavazzoni, D. Ceresoli, M. Cococcioni, N. Colonna, I. Carnimeo, A. Dal Corso, S. de Gironcoli, P. Delugas, R.A. DiStasio, A. Ferretti, A. Floris, G. Fratesi, G. Fugallo, R. Gebauer, U. Gerstmann, F. Giustino, T. Gorni, J. Jia, M. Kawamura, H.-Y. Ko, A. Kokalj, E. Küçükbenli, M. Lazzeri, M. Marsili, N. Marzari, F. Mauri, N.L. Nguyen, H.-V. Nguyen, A. Otero-de-la-Roza, L. Paulatto, S. Poncé, D. Rocca, R. Sabatini, B. Santra, M. Schlipf, A.P. Seitsonen, A. Smogunov, I. Timrov, T. Thonhauser, P. Umari, N. Vast, X. Wu, S. Baroni, Advanced capabilities for materials modelling with Quantum ESPRESSO, J. Phys.: Condens. Matter 29 (2017) 465901, https://doi.org/10.1088/1361-648X/aa8f79.

[30] K.F. Garrity, J.W. Bennett, K.M. Rabe, D. Vanderbilt, Pseudopotentials for high-throughput DFT calculations, Comput. Mater. Sci. 81 (2014) 446–452, https://doi.org/10.1016/J.COMMATSCI.2013.08.053.

[31] J.P. Perdew, K. Burke, M. Ernzerhof, Generalized gradient approximation made simple, Phys. Rev. Lett. 77 (1996) 3865–3868, https://doi.org/10.1103/PhysRevLett.77.3865.

[32] S. Grimme, Semiempirical GGA-type density functional constructed with a long-range dispersion correction, J. Comput. Chem. 27 (2006) 1787–1799, https://doi.org/10.1002/jcc.20495.

[33] V. Barone, M. Casarin, D. Forrer, M. Pavone, M. Sambi, A. Vittadini, Role and effective treatment of dispersive forces in materials: polyethylene and graphite crystals as test cases, J. Comput. Chem. 30 (2009) 934–939, https://doi.org/10.1002/jcc.21112.

[34] J.V. Barth, H. Brune, G. Ertl, R.J. Behm, Scanning tunneling microscopy observations on the reconstructed Au(111) surface, Phys. Rev. B 42 (1990) 9307–9318.

[35] E.V. Iski, A.D. Jewell, H.L. Tierney, G. Kyriakou, E.C.H. Sykes, Controllable restructuring of a metal substrate: tuning the surface morphology of gold, Surf. Sci. 606 (2012) 536–541, https://doi.org/10.1016/j.susc.2011.11.028.

[36] E. Cariati, E. Lucenti, A. Previtali, A. Forni, Cyclic triimidazole derivatives: an intriguing family of multifaceted emitters, handbook of aggregation-induced Emission, Typical Aiegens Desig. 2 (2022) 165–193.

[37] Y. Bian, J. Cheng, Y. Zhang, H. Sun, J. Zhang, X. Zhang, Q. Jin, Herringbone reconstruction-mediated assembly of 2-(Hydroxymethyl)benzimidazole molecules on Au(1 1 1) studied by scanning tunneling microscope, Chem. Phys. Lett. 803 (2022) 139799, https://doi.org/10.1016/j.cplett.2022.139799.

[38] M. Magni, E. Lucenti, A. Previtali, P.R. Mussini, E. Cariati, Electrochemistry of cyclic triimidazoles and their halo derivatives: a casebook for multiple equivalent centers and electrocatalysis, Electrochim. Acta 317 (2019) 272–280, https://doi.org/10.1016/j.electacta.2019.05.146.

[39] Y. Takeuchi, K.L. Kirk, L.A. Cohen, Imidazole cyclotrimers (trimidazoles), a novel heteroannular series, J. Org. Chem. 44 (1979) 4243–4246, https://doi.org/10.1021/jo01338a006.

[40] G.-J. Su, H.-M. Zhang, L.-J. Wan, C.-L. Bai, T. Wandlowski, Potential-induced phase transition of trimesic acid adlayer on Au(111), J. Phys. Chem. B 108 (2004) 1931–1937, https://doi.org/10.1021/jp035095g.

[41] Z. Li, K. Mali, P. Hapiot, S. De Feyter, A.-J. Attias, S.F.L. Mertens, Reversible redox-driven crystallization in a paracyclophane monolayer at a solid–liquid interface, Adv. Funct. Mater. 34 (2024) 2315861, https://doi.org/10.1002/adfm.202315861.

[42] S. Yoshimoto, T. Kawamoto, T. Okawara, Y. Hisaeda, M. Abe, Conformational change in molecular assembly of nickel(II) tetra(n-propyl)porphycene triggered by

potential manipulation, Langmuir 32 (2016) 13635–13639, https://doi.org/10.1021/acs.langmuir.6b03782.
[43] S. Yoshimoto, J. Inukai, A. Tada, T. Abe, T. Morimoto, A. Osuka, H. Furuta, K. Itaya, Adlayer structure of and electrochemical O2 reduction on cobalt porphine-modified and cobalt octaethylporphyrin-modified Au(111) in HClO 4, J. Phys. Chem. B 108 (2004) 1948–1954, https://doi.org/10.1021/jp0366421.
[44] L. Bardini, M. Ceccato, M. Hinge, S.U. Pedersen, K. Daasbjerg, M. Marcaccio, F. Paolucci, Electrochemical polymerization of allylamine copolymers, Langmuir 29 (2013) 3791–3796, https://doi.org/10.1021/la304766k.
[45] P. Zelenay, P. Waszczuk, K. Dobrowolska, J. Sobkowski, Adsorption of benzoic acid on a polycrystalline gold electrode, Electrochim. Acta 39 (1994) 655–660, https://doi.org/10.1016/0013-4686(94)80007-3.